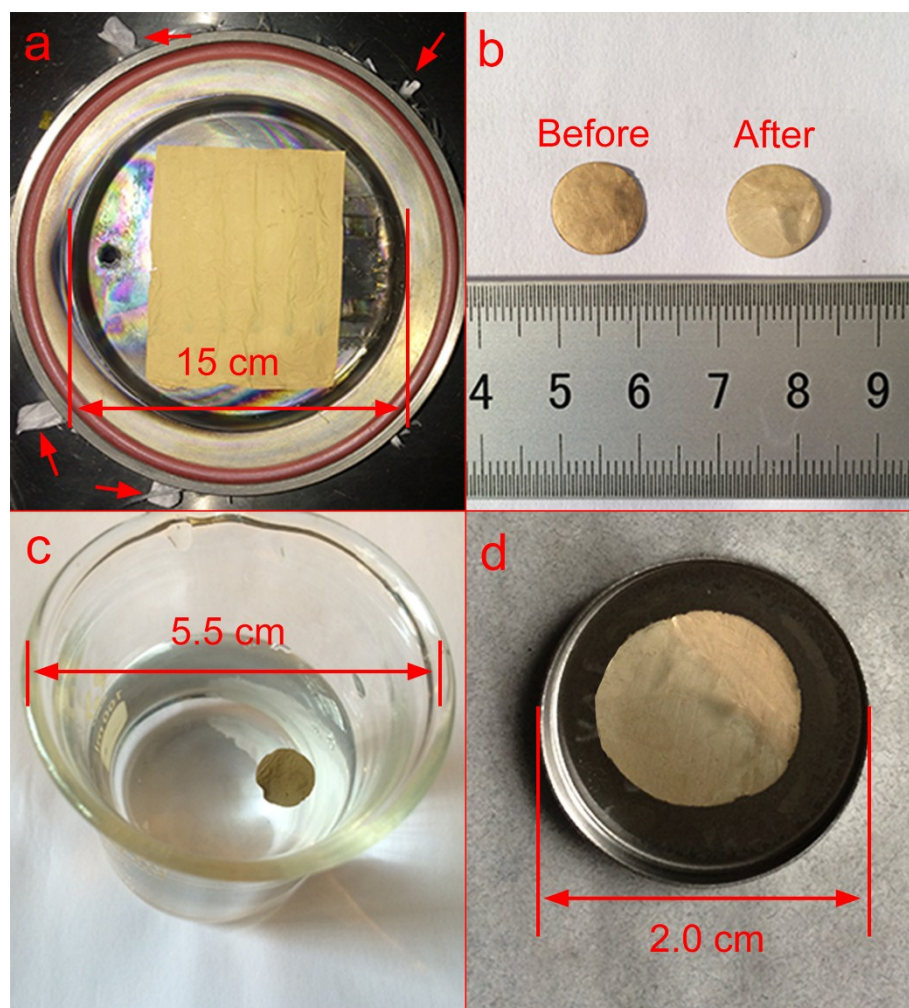
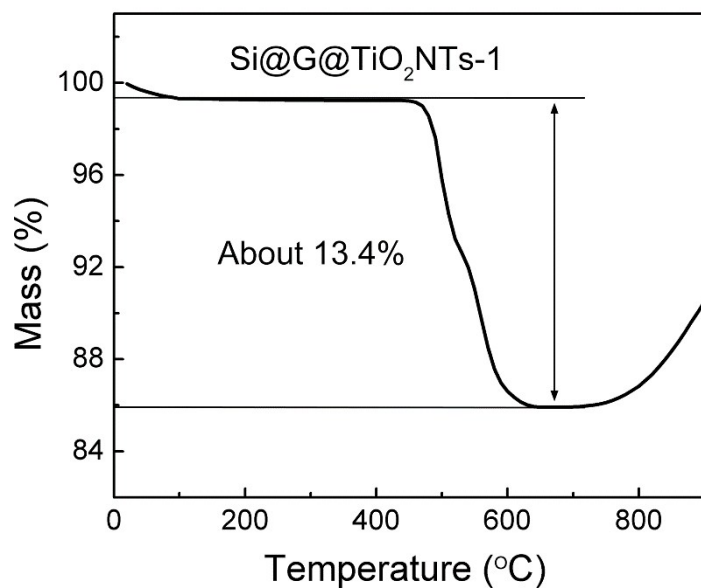


## Electronic Supplementary Information

### Large-scale production of silicon nanoparticles@graphene embedded in nanotubes as ultra-robust battery anodes



**Fig. S1** (a) Image of as-electrospun Si@G@PVP NFs membrane in the homemade hot-wall closed chamber type atomic layer deposition (ALD) system. Red arrows mark is heater band. (b) Digital photo of as-punched Si@G@PVP NFs membrane (left) before and (right) after being coated amorphous TiO<sub>2</sub>, the color of the membrane change a little after 200 ALD cycles. (c) Image of as-punched membrane soaked in water, indicating the membrane can remain an integrated morphology after washing. (d) Image of the free-standing membrane anode after washing and drying on the battery case.



**Fig. S2** TGA curve of Si@G@TiO<sub>2</sub>NTs-1. The content of graphene can be directly calculated about 13.4% from the curve. The mass ratio of SiNPs and graphene is 4:1 in precursor solution, suggesting the content of SiNPs can be calculated about 53.6% in the whole composite.

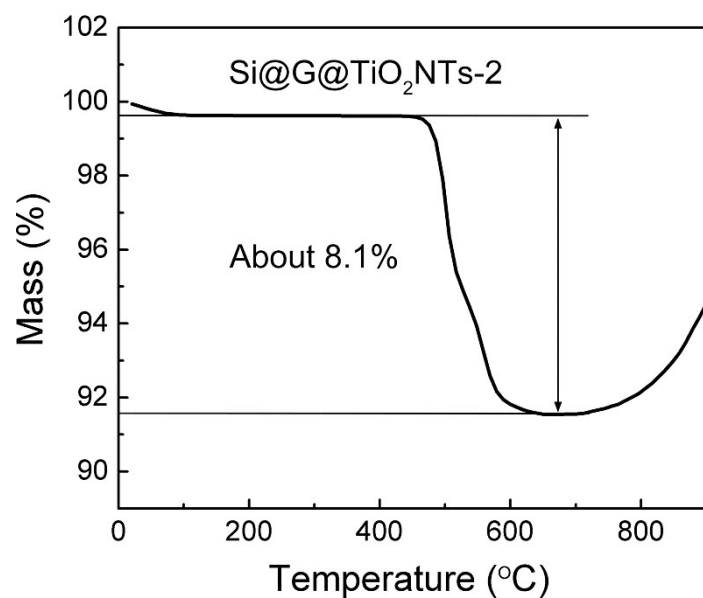


**Fig. S3** TGA curve of Si@G@TiO<sub>2</sub>NTs-2. The mass ratio of SiNPs and graphene is 8:1 in precursor solution, indicating the content of SiNPs is about 64.8% in the whole composite, and the rest of mass fraction about 27.1% can be ascribed to TiO<sub>2</sub>NTs.

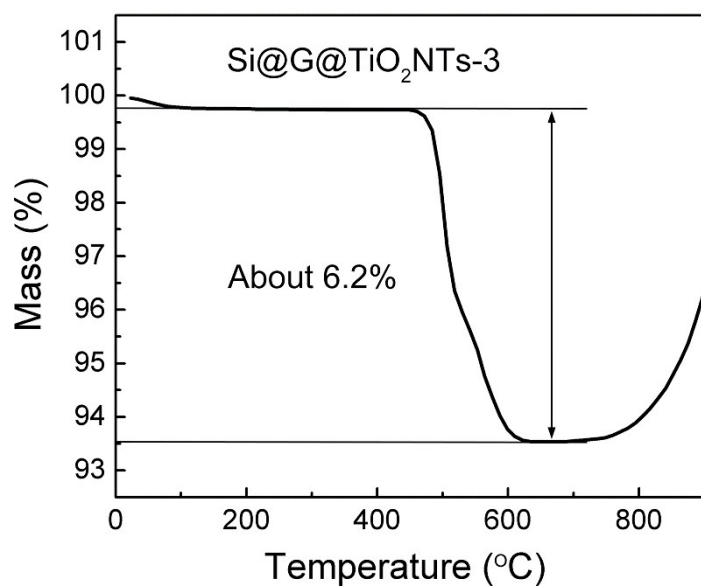


**Fig. S4** TGA curve of Si@G@TiO<sub>2</sub>NTs-3. The mass ratio of SiNPs and graphene is 12:1 in precursor solution. So the mass fraction of SiNPs can be calculated about 74.4% in the whole composite.

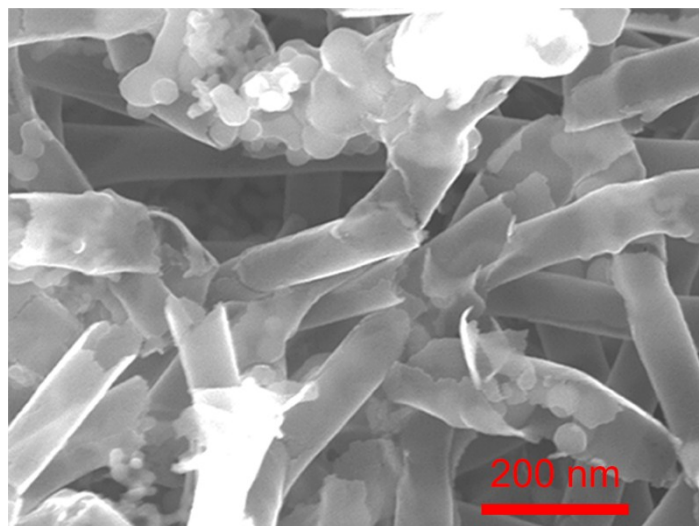


**Fig. S5** SEM image of Si@G@TiO<sub>2</sub>NTs-3 after 100 cycles, indicating that too high content of SiNPs would burst TiO<sub>2</sub>NTs.

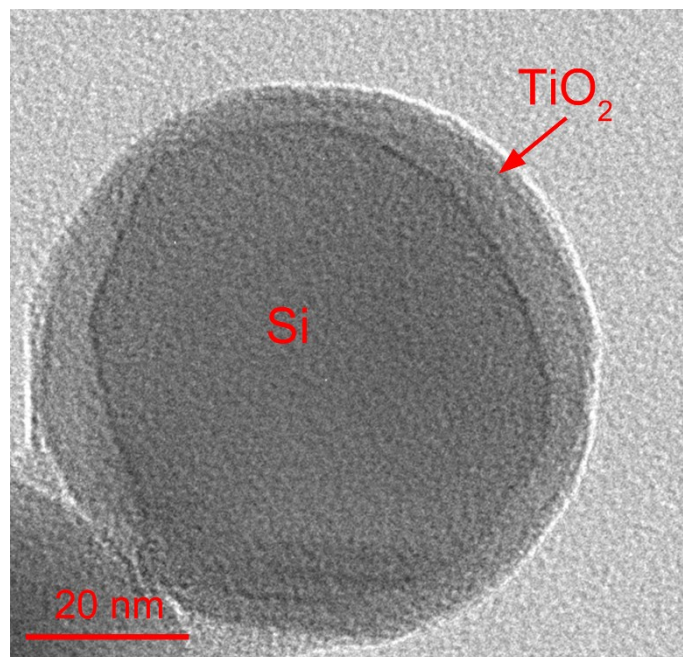


**Fig. S6** TEM image of SiNPs directly coated TiO<sub>2</sub> without void space and graphene. The electrode shows a bad cyclic performance and delivers a relatively low capacity, which is attributed to the huge volume change and poor electrical conductivity of Si during the cyclic process.

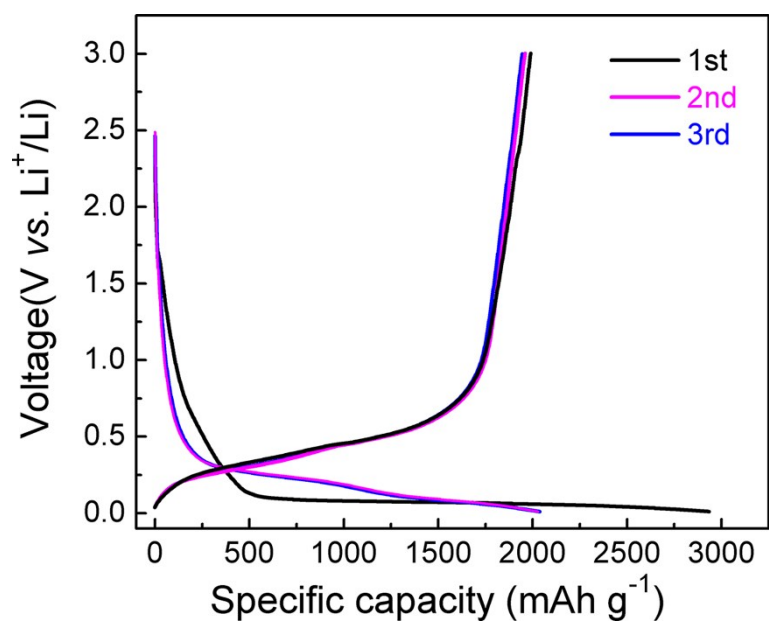


**Fig. S7** Charge and discharge profiles of Si@G@TiO<sub>2</sub>NTs obtained in the 1st, 2nd and 3rd cycles.

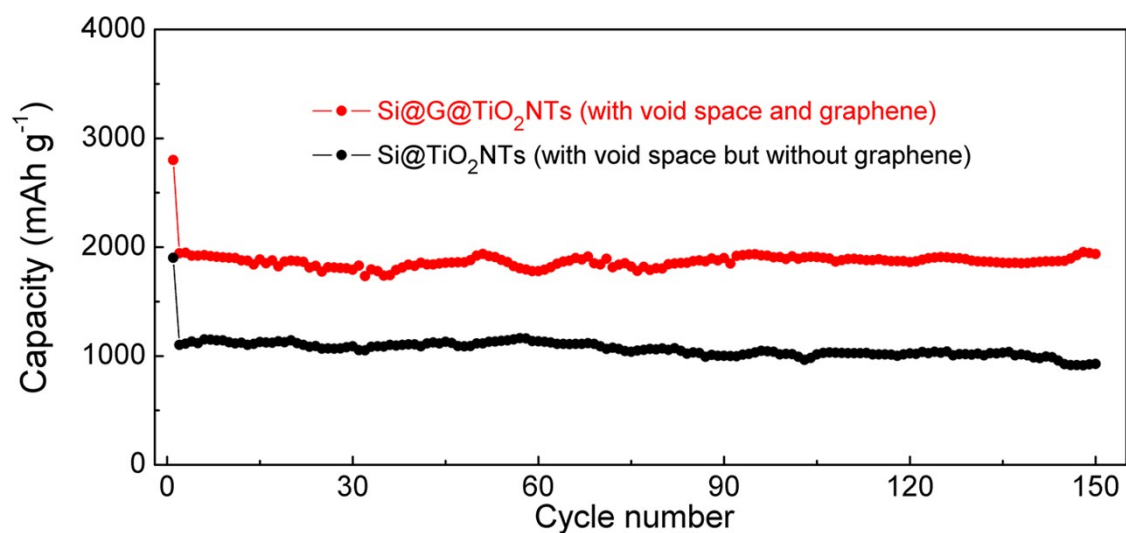


**Fig. S8** Cyclic performance of Si@G@TiO<sub>2</sub>NTs (with void space and graphene) and Si@TiO<sub>2</sub>NTs (with void space but without graphene). It clearly showed a higher capacity can be obtained when the absence of graphene than that without graphene. The graphene conductive networks embedded in nanotubes increased the contact between the silicon nanoparticles and nanotubes, enabled every Si nanoparticle was involved in the electrochemical reaction, leading to a superior capacity.



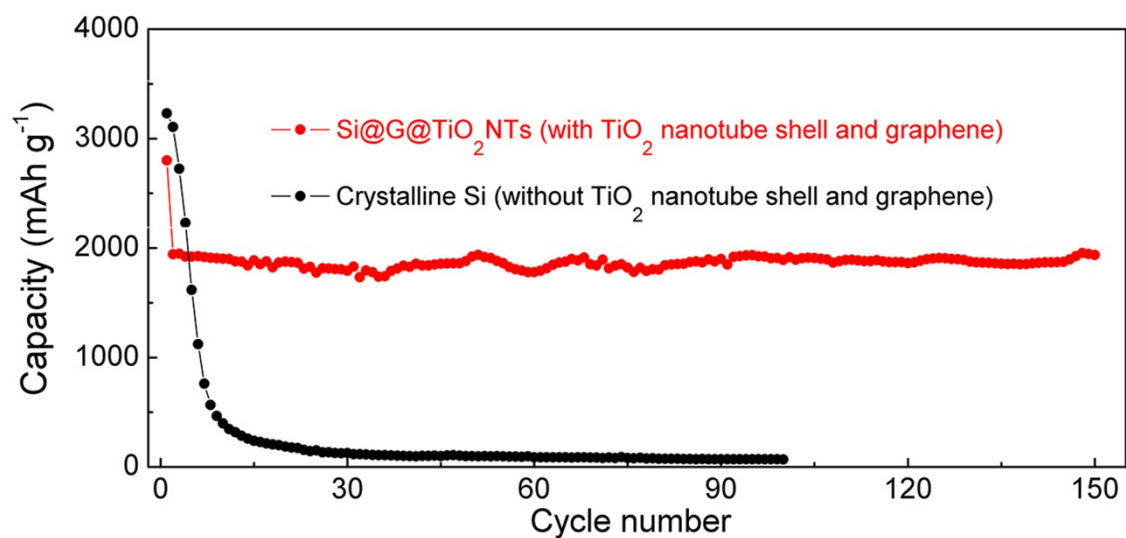


**Fig. S9** Cycling performance of Si@G@TiO<sub>2</sub>NTs (with TiO<sub>2</sub> nanotube shell and graphene) and crystalline Si (without TiO<sub>2</sub> nanotube shell and graphene). This clearly can be seen that the TiO<sub>2</sub> nanotube shell greatly improve the cyclic performance of Si-based anodes.

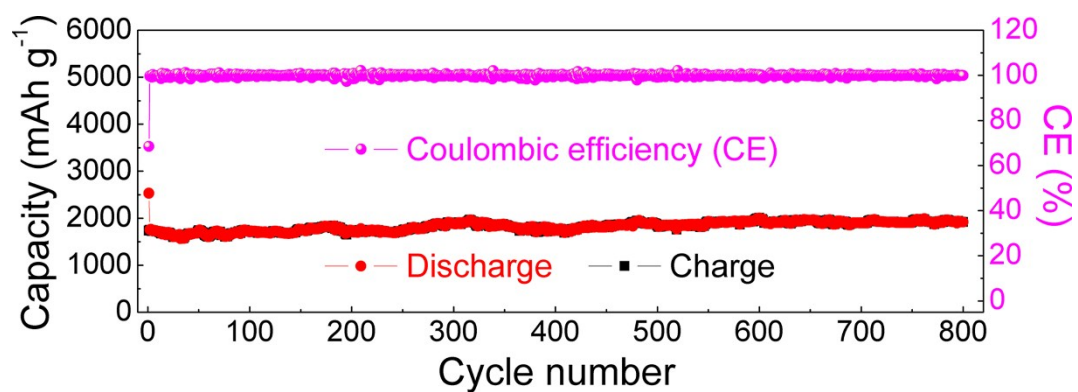


**Fig. S10** Cyclic performance and Coulombic efficiency of Si@G@TiO<sub>2</sub>NTs-2 anode. It is worth noting that the electrode still shows a high capacity of 2226.4 mAh g<sup>-1</sup> after 800 cycles. Moreover, the average Coulombic efficiency is calculated as 99.94% during the 800 cycles.

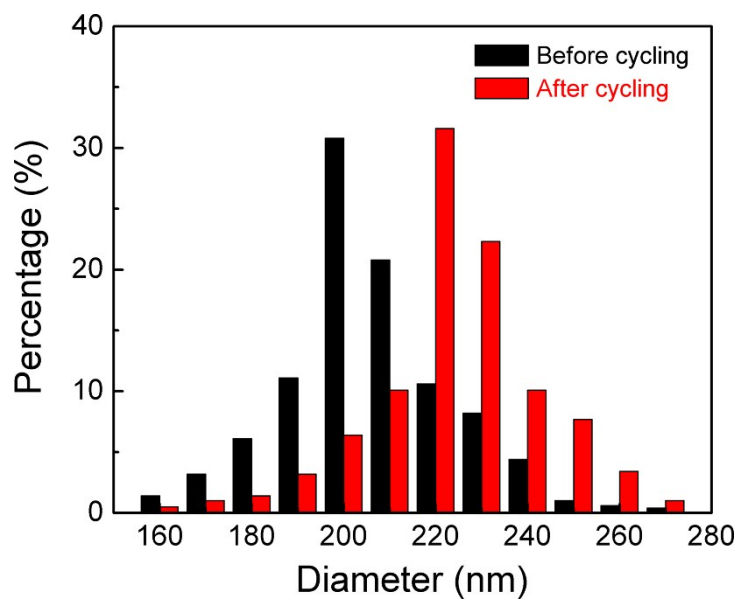


**Fig. S11** The diameter distribution of TiO<sub>2</sub>NTs before and after 100 deep cycles, the average diameter of the nanotubes increases only about 18 nm, which is attributed to the formation of the stable and thin SEI.

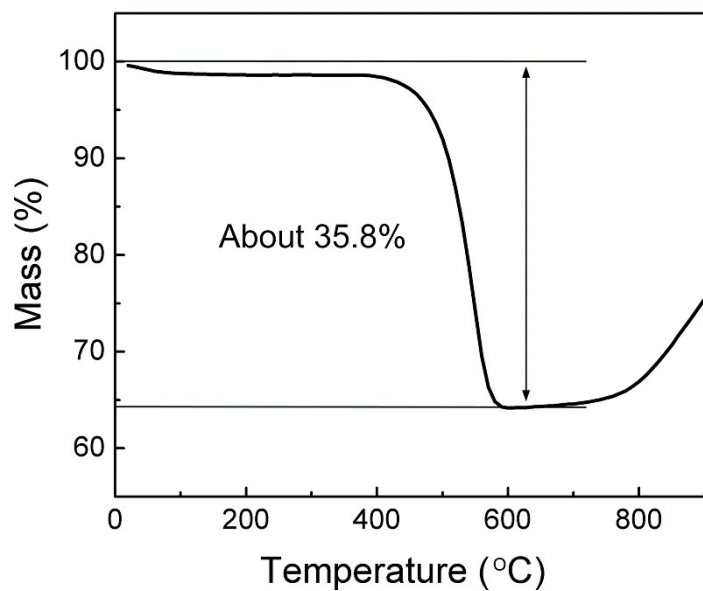


**Fig. S12** TGA curve of as-prepared Si@G@CNTs. The content of SiNPs is calculated about 64.2% in the whole composite.